Design and Testing of a Hall Effect Thruster with 3D Printed Channel and Propellant Distributor

IEPC-2017-119

Presented at the 35th International Electric Propulsion Conference
Georgia Institute of Technology • Atlanta, Georgia • USA
October 8 – 12, 2017

Ethan P. Hopping[1] and Kunning G. Xu[2]
Department of Mechanical and Aerospace Engineering, University of Alabama in Huntsville, Huntsville, Alabama, 35816, United States

The UAH-78AM is a low-power Hall effect thruster developed at the University of Alabama in Huntsville with channel walls and a propellant distributor manufactured using 3D printing. The goal of this project is to assess the feasibility of using unconventional materials to produce a low-cost functioning Hall effect thruster and consider how additive manufacturing can expand the design space and provide other benefits. A version of the thruster was tested at NASA Glenn Research Center to obtain performance metrics and to validate the ability of the thruster to produce thrust and sustain a discharge. An overview of the thruster design and transient performance measurements are presented here. Measured thrust ranged from 17.2 mN to 30.4 mN over a discharge power of 280 W to 520 W with an anode I_{SP} range of 870 s to 1450 s. Temperature limitations of materials used for the channel walls and propellant distributor limit the ability to run the thruster at thermal steady-state.

Nomenclature

ABS	=	acrylonitrile butadiene styrene
BaO	=	barium oxide
FFF	=	fused filament fabrication
GRC	=	Glenn Research Center
HET	=	Hall effect thruster
I_{SP}	=	specific impulse, s
T	=	thrust, mN
sccm	=	standard cubic centimeters per minute, cm^3/min
SEE	=	secondary electron emission
SEM	=	scanning electron microscope
VF-8	=	Vacuum Facility-8

I.Introduction

THE current drivers of cost and manufacturing time with Hall effect thrusters are fabrication of the anode and channel assemblies. In most Hall thrusters, the propellant distributor is integrated into the anode assembly, necessitating manual fabrication and welding processes to integrate the baffle assemblies, orifices, and other distributor assemblies into the anode. Furthermore, the channel assemblies of most Hall thrusters are manufactured from boron nitride, a hot-pressed ceramic that must be subtractively machined to obtain the annular channel geometry. Monolithic boron nitride dimensions are currently limited by the hot-pressing process, and this poses

[1] Graduate Research Assistant, Mechanical and Aerospace Engineering, AIAA Student Member.
[2] Assistant Professor, Mechanical and Aerospace Engineering, AIAA Senior Member.

challenges for the design of large thrusters [1,2]. In addition, the cost of the boron nitride components increases substantially with thruster size.

In other aerospace industries, additive manufacturing, or colloquially 3D printing, is being leveraged to dramatically reduce the cost of component fabrication as compared to conventional methods[3]. Propulsion systems are particularly well suited to benefit from additive manufacturing processes due to the complex geometry and low-volume production. The objective of this research is to investigate applications of additive manufacturing to reduce the cost of Hall effect thruster fabrication—with a specific focus on low-cost, fast turnaround, and high availability processes. Additive manufacturing enables design simplifications that can potentially reduce Hall Thruster manufacturing cost and time. Once such significant design simplification that can be realized is 3D printing of the channel and direct integration of the propellant distributor into the channel. This not only reduces part count for the propellant distribution system, but also eliminates the baffle and orifice geometry that is traditionally integrated into the anode. Furthermore, 3D printing enables components to be manufactured and replaced at low-cost. This enables test programs to investigate multiple geometries that would be cost prohibitive to manufacture using traditional methods and materials.

However, the material requirements for Hall effect thrusters are stringent due to high steady-state operating temperatures and unique secondary electron emission requirements for channel materials. In SPT-type Hall thrusters, the high SEE of the channel wall material is necessary to reduce plasma electron temperature, which increases ionization efficiency[4–6]. This limits material selection to dielectrics with high SEE coefficients as compared to metals. Boron nitride is an ideal choice in conventionally-manufactured thrusters; however, 3D printing of refractory ceramics is still its nascence and currently limited in terms of build volume, component detail, and availability. It is expected that polymers provide SEE profiles similar to ceramics, but they also present design challenges due to low melting temperatures. However, the broad availability and low-cost of 3D printing processes using polymers made them a good choice for the proof-of-concept in this work.

II. Experimental Setup

A. Thruster

1. Overview

To research applications for the use of low-cost additive manufacturing in the design of Hall thrusters, we designed an SPT-type Hall thruster to use as a test bed for different channel designs and materials. The UAH-78AM is the first Hall Thruster to be developed at The University of Alabama in Huntsville (UAH). Several images of the thruster are provided in Fig. 1, and an isometric view of the design tested at GRC is provided in Fig. 2.

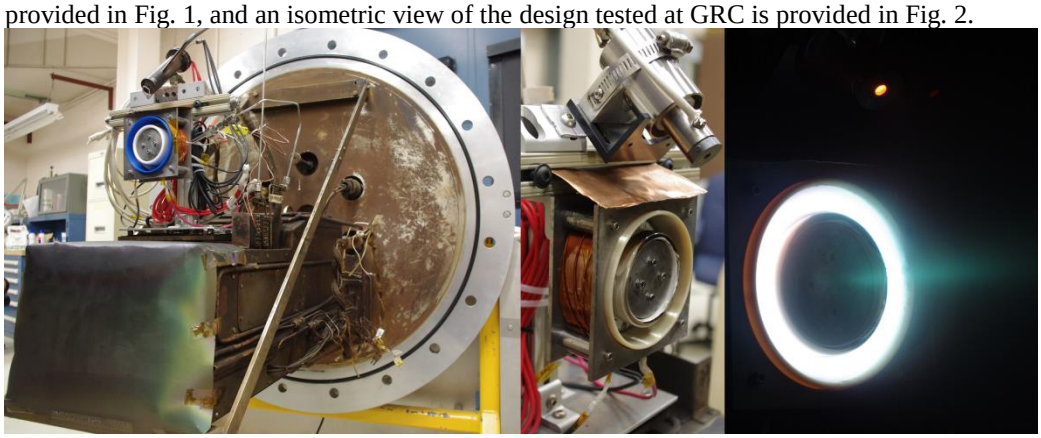

Fig. 1 Testing of the UAH-78AM

The UAH-78AM was designed to fit in CubeSat dimensions for demonstration purposes and to facilitate testing in small vacuum facilities. The dimensions were chosen based on a loose scaling of the channel and magnetic field topology of the P5 HET[7]. However, the discharge power of 300-500 W is well above the power supply capabilities of most CubeSats. The higher discharge power was chosen because Hall thrusters small enough to be powered by CubeSats currently have significant channel wall erosion and electron losses due to the increased surface to volume ratio[8].

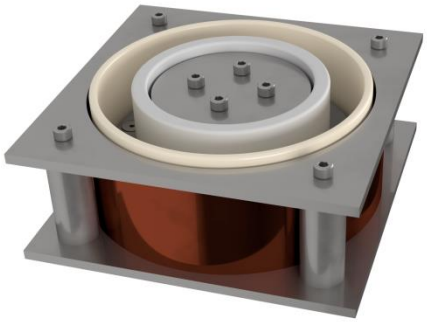

Fig. 2 3D rendering of UAH-78AM configuration as tested at GRC

2. 3D Printed Components

Components selected for 3D printing included the channel and propellant distributor. Initially, these two parts were printed as a monolithic component to reduce part count. The propellant distributor was integrated into the base of the channel. The printed propellant distributor allowed us to use a simple stainless steel ring as the anode, thus separating propellant injection from the anode. Initial testing revealed that the lifetime limiting component in the thruster was the channel, which would degrade due to heating near the channel exit plane. Therefore, later versions of the thruster separated the channel from the propellant distributor, simplifying thruster disassembly and enabling the channels to be replaced without reprinting the propellant distributor. Separating the channel from the propellant distributor also allowed the channel to be printed from a higher-temperature thermoplastic such as ULTEM in order to improve lifetime.

The additive manufacturing process presents challenges in terms of part tolerance and minimum feature size. Part tolerances and accuracy are difficult to quantify with many 3D printing processes because they are frequently geometry dependent. Accuracy limitations were most apparent for the 3D printed glazed ceramic. The 3D printed ceramic is not hot-pressed, and therefore undergoes a firing and glazing process after printing to reach the finished state. The firing process induces part shrinkage on the order of 3% of total part size and must be accounted for in the design. In addition, minimum feature size is limited to approximately 2 mm. The ceramic process was not considered for the propellant distributor due to the more stringent tolerances required for the part.

Separate 3D printers were used for the ULTEM outer channel and ABS propellant distributor. Part accuracy for the ULTEM printer is ±0.130 mm or better. Accuracy for the ABS 3D printer is more difficult to predict as this was not a commercial 3D printer. Therefore, factors such as belt backlash and part shrinkage are not taken into account when quoting accuracy. However, axis resolution is 0.01mm, and since the 3D printing technology is functionally identical to the ULTEM 3D printer, part accuracy is likely comparable. The smallest features in our parts were the propellant distributor orifices, which had a diameter of .01 in (0.254 mm). Light sanding was used for part cleanup on polymer components in some areas to improve fit.

Future revisions of the thruster may explore applications for 3D printing in the design of the magnetic circuit. However, at this time 3D printing of magnetic components is still an emerging technology with limited availability. Furthermore, many 3D printed magnet processes currently are focused on polymer-bonded magnets[9,10]. Bonded magnets generally have lower maximum energy product than metallic magnets[11], thus requiring larger magnets to produce required magnetic field intensities.

3. Cost and Turnaround Time

Table 1 provides a cost breakdown for the UAH-78AM, in USD. All materials for the thruster in the United States can be procured for a total of $300 or less. This cost assumes the availably of 3D printers and other equipment. The low cost makes manufacturing the thruster accessible to most education and research programs.

Table 1: UAH-78AM cost breakdown

Material	Component	Cost	Notes
Carbon Steel	Magnetic Circuit	$ 57	
Fasteners	Magnetic Circuit	$ 30	
Magnet Wire	Magnetic Circuit	$ 30	
Carbon Shim Stock	Magnetic Shields	$ 15	
Stainless Steel	Anode	$ 4	Fabricated from stainless steel washer
3D printed glazed ceramic	Inner Channel	$ 21	Quote from manufacturer
ULTEM	Outer Channel	$ 97	Quote from manufacturer
ABS	Inner Channel	$ 2	By Volumetric Material Cost
Material Total		**$ 256**	
Labor		$ 560	35 $/hr for 16 hrs
Total		**$ 816**	

Costs for the ULTEM outer channel and glazed ceramic inner channel are based on quotes directly from 3D printer suppliers. Consequently, these costs are significantly inflated as compared to the true costs of materials and print time. It is increasingly common for academic institutions to have access to 3D printing services on campus or through business partnerships. These services frequently provide print services at material cost or less, so it is possible that the inner and outer channel components could be procured for much lower cost. ABS 3D printing is so broadly available through professional and hobbyist services that we provide the component price based on volumetric material cost.

The most significant labor costs are in fabrication of the magnetic circuit, which is cut using a conventional machining process. However, significant efforts were made in the design of the thruster to simplify machining operations as much as possible. Machining for the magnetic circuit is dominated by hole processes. While access to CNC machining simplifies manufacturing, all parts could be produced with relative ease using manual machines. The authors estimate that total labor time for a skilled machinist on magnetic circuit fabrication would be a day or two. However, labor remains the costliest portion of UAH-78AM procurement assuming a machinist pay of $ 35 per hour.

In comparison, a first order cost estimate is provided for producing the UAH-78 using conventional methods in Table 2.

Table 2: UAH-78AM cost breakdown (conventional materials)

Material	Component	Cost	Notes
Carbon Steel	Magnetic Circuit	$ 57	
Fasteners	Magnetic Circuit	$ 30	
Magnet Wire	Magnetic Circuit	$ 30	
Carbon Shim Stock	Magnetic Shields	$ 15	
Stainless Steel	Anode	$ 50	Thicker stock material to incorporate distributor geometry
Boron Nitride Channel	Discharge Channel	$ 1060	Scaled from larger thruster. Includes Labor
Material Total		**$ 1242**	
Labor		$ 3800	35 $/hr for 10 days, anode and magnetic circuit fabrication + $ 1000 for orifice drilling
Total		**$ 5042**	

The drivers of cost in this estimate are the labor costs associated with anode fabrication and the boron nitride channel. For the anode, more time is required for the machining and welding associated with integrating the propellant distributor. Likewise, a significant increase in machining time is incurred for fabrication of the channel. The requirement for more skilled labor time causes the conventionally manufactured UAH-78AM to be more expensive than the 3D printed thruster by over a factor of 6. This example suggests that a significant cost reduction

associated with 3D printing is incurred by reducing the skilled labor costs associated with manufacturing the thruster.

Because the channel and propellant distributor are produced additively, all other labor costs are associated with manual assembly. Experience from testing demonstrates that the thruster can be assembled from raw components in a week or less. In addition, the turnaround time for servicing between tests is on the order of a couple of days.

B. Cathode

A BaO cathode was used with a fixed flow rate of 0.5 mg/s for all tests. The cathode was oversized for the anode current required to sustain thruster discharge. Consequently, the discharge current was too low to allow for self-heating, thus requiring the cathode heater to run at half-power during tests to ensure stable operation. Since cathode flow is not optimized, all specific impulses are presented in terms of the anode flow. It is likely that cathode flow could be reduced to 6-7% of anode flow while maintaining stable discharge.

C. Test Facility

Tests were conducted in Vacuum Facility 8 at NASA Glenn Research Center. The main chamber of VF-8 has a diameter of 1.5m and a length of 4.5m. Pumping is provided by four oil-diffusion pumps with a speed of 1.2×10^5 liters per second at 10^{-5} torr [12]. VF-8 features two bell-jars that can be independently isolated from the main chamber using gate valves. The thruster was mounted on an inverted-pendulum thrust stand attached to the vacuum flange of the primary bell jar. The design and operation of this type of thrust stand is well established in literature, and further details on the design of similar stands at Glenn are provided in [13].

Anode and cathode propellant flow were provided by 100 sccm and 25 sccm mass flow controllers manufactured by Celerity, and all tests were run using Xenon. No ion or plume data were collected due to the short duration of tests.

D. Test Matrix

Our focus with the UAH-78AM was on operation at low-power and discharge voltage that could be sustained by small satellites. Furthermore, the low service temperatures of materials used in the propellant distributor and discharge channel limited operation at higher power due to higher channel wall heating rates associated with high-power operation[14]. The testing at GRC focused on identifying stable low-voltage operating points and flow rates and obtaining baseline performance parameters. It was found that 200 V and 1.82 mg/s anode flow produced a stable discharge at our chosen magnet settings. The objective was to run the thruster at operating points barely in the jet mode of Hall thruster discharge, where efficiency is significantly improved from a diffuse mode but power requirements remain low[15]. Therefore, once the 200 V operating point was identified, discharge voltage was incremented by 20 V from 180-260 V, and anode flow was incremented by 0.18 mg/s between 1.64 and 2.18 mg/s.

Initial thrust measurements were taken in 5 second test intervals to limit thruster heating. After the 5 second data were collected for our test matrix, the operating time was increased to 15 seconds to get closer to steady-state behavior. Several thrust measurements were taken over longer durations on the order of 30 seconds to assess thrust stability in longer tests.

III.Results

A. Overview

The presence of polymer components in our thruster presents unique challenges for quantifying baseline performance. Not only were we unable to run the thruster long enough to get through the transitional regime associated with conventional thruster start-up, but the heating of the polymer components limited testing duration to approximately 30 seconds. Beyond 30 seconds, a failure mode is observed where a hotspot attaches to the outer ULTEM discharge channel wall and the thruster enters a current-limited mode of operation.

Without the ability to operate the thruster at steady-state, we choose to characterize performance by comparing thrust and specific impulse at fixed times after ignition. The ignition event is identified through a derivative approach. The derivative is taken of the thrust trace and time zero is identified as the location where the thrust rate of change exceeds 20 mN/sec, as this behavior is only seen during thruster ignition. For the 5 second tests, thrust and specific impulse are measured 4 seconds after the ignition event. For 15 second tests, measurements are taken 14 seconds after ignition. We expect thruster thermal conditions to be similar at fixed times after ignition, enabling comparison across different discharge voltages and flow rates. However, the heating rate and thermal condition of

the channel likely varies between tests, resulting in some error in repeatability. We attempt to characterize this uncertainty through repeated tests. Calibration and measurement uncertainties associated with the equipment are calculated and reported according to the best practices identified in Ref [16,17]. While thrust and I_{SP} uncertainty vary slightly with the calibration for each test run, the average thrust uncertainty at 95% confidence is ±0.72 mN, and I_{SP} uncertainty is ±40 sec.

B. Thrust

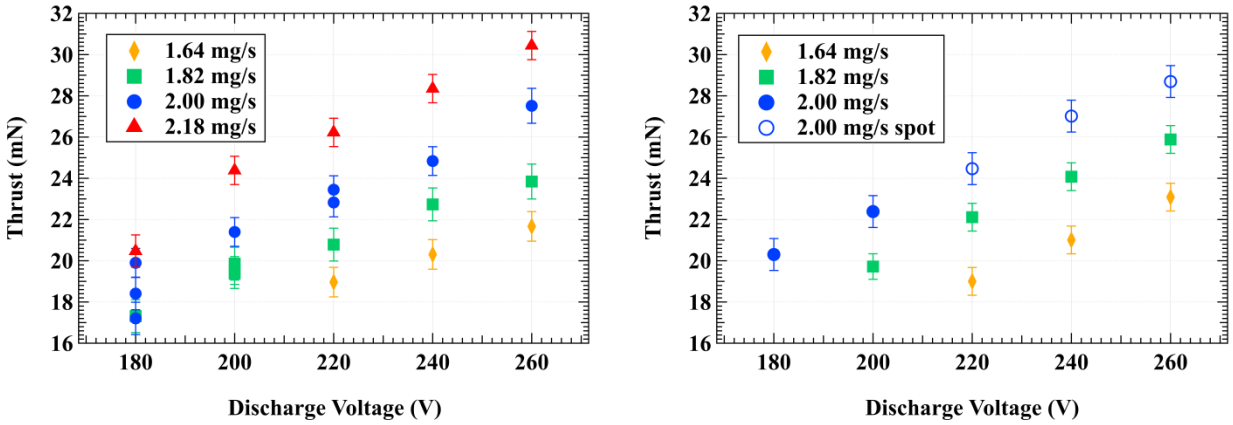

Fig. 3 Thrust as a function of discharge voltage from 5 second tests (left) and 15 second tests (right)

Fig. 3 provides measured thrust as a function of discharge voltage for the 5 and 15 second test runs. General trends are as expected for conventional Hall thrusters, with thrust increasing with both discharge voltage and flow rate. Measured thrust ranges from 17.2 mN to 30.4 mN.

Repeat tests are visible in the 5 second data at 180, 200, and 220 V operating points. At 180V, the 2.00 mg/s repeat tests display a vertical spread of approximately 5 mN, and the error bounds do not account for the differences in measured thrust. During testing it was noted that the thruster took longer than normal to start and for the discharge to settle at this operating point. It is suspected that the 180 V operating point is at the lower limit of jet-mode discharge with our magnet settings for 2.00 mg/s flow rate, resulting in poor stability. Repeat tests at 200 and 220 V fall within the uncertainty of our equipment, demonstrating that the short duration tests can yield consistent measurements at higher voltages. The thruster could not be started at 1.64 mg/s and 180 or 200 V without adjusting magnet settings, thus and no data were collected at these operating points.

While collecting 15 second data at 220 V and 2.00 mg/s, a spot formed and attached to the outer channel wall. Affected tests are labeled in all plots with hollow circles. The damage associated with spot formation on the outer channel could change the efficiency of the thruster by increasing anode leakage current, limiting comparisons with preceding operating points. However, the data points are included for completeness since we were able to start and run the thruster without visible spotting behavior after the channel had been allowed to cool. Furthermore, no 15 second measurements were made at 2.18 mg/s due to the spot formation. The channel wall heating rate increases at higher discharge powers, which are associated with higher flow rates [14]. To avoid further spotting damage to the outer channel, we decided to forgo longer duration testing at the higher discharge powers associated with the 2.18 mg/s flow rate.

C. Anode Specific Impulse

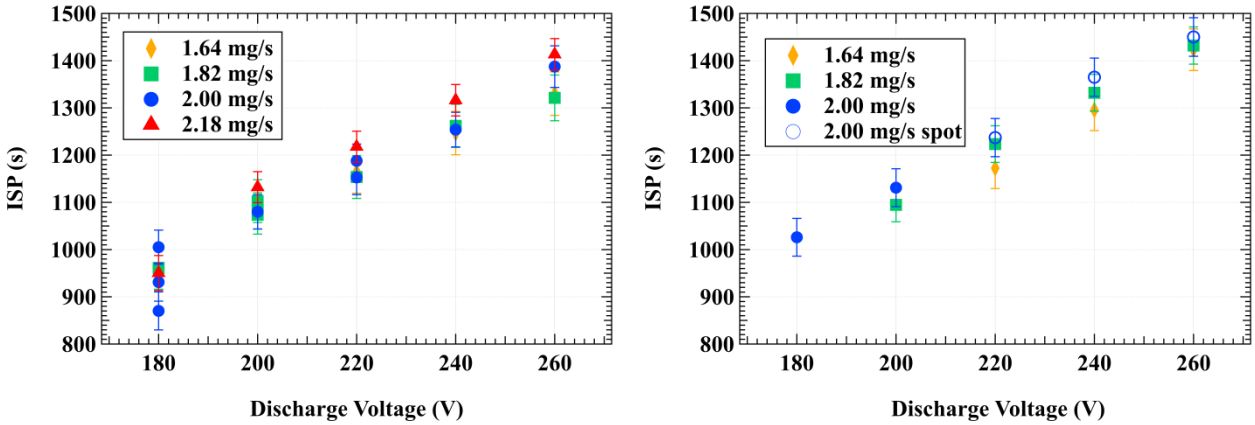

Fig. 4 Anode Specific Impulse as a function of discharge voltage for 5 second tests (left) and 15 second tests (right)

Fig. 4 provides anode specific impulse as a function of discharge voltage. The anode specific impulse ranges from 870 to 1,450 seconds and increases with discharge voltage, which is a normal behavior for Hall thrusters. The data also suggest that specific impulse increases with flow rate in our test matrix; however, due to equipment uncertainty this correlation cannot be proven from the data.

D. Anode Efficiency

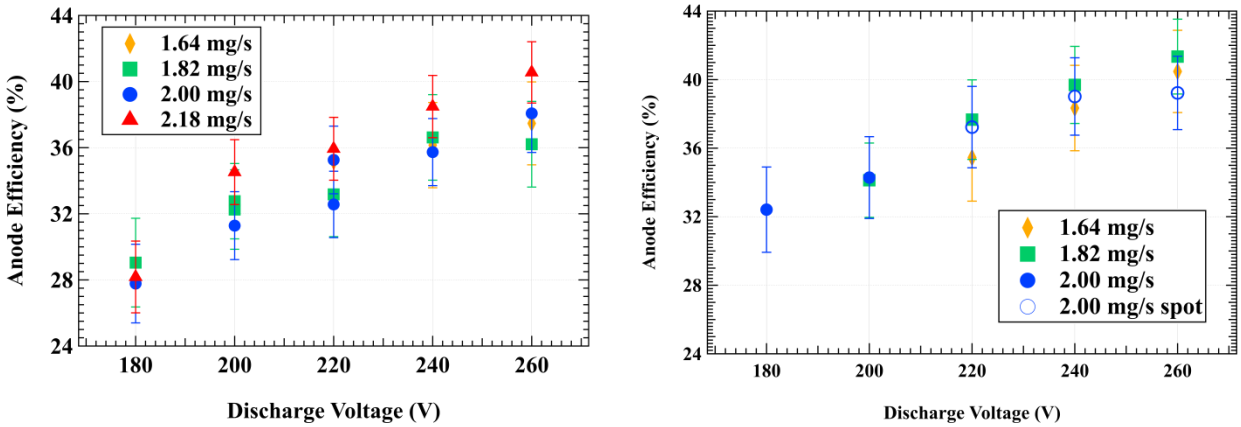

Fig. 5 Anode efficiency as a function of discharge voltage for 5 second tests (left) and 15 second tests (right)

Fig. 5 provides anode efficiency as a function of discharge voltage. Anode efficiency generally increases as a function of discharge voltage and ranges from 27.8% to 42.2%. At 260 V and anode flow of 2.00 mg/s, the anode efficiency decreases relative to the 240 V operating point in the 15 second tests. This measurement was taken after initial formation of the spot on the outer channel wall. The decrease in anode efficiency may be a product of increased anode leakage current due to the damage to the outer channel wall. It was noted in testing that discharge current increased relative to the 5 second tests after formation of the spot, which would be expected if the damage from spotting were reducing thruster performance.

The effect of anode flow on thruster efficiency is unclear from the data due to uncertainty. In the 15 second tests, it appears that the 1.64 mg/s flow rate results in higher efficiencies at discharge voltages above 200 V, while 2.00 mg/s is more efficient at the lower voltages. The 5 second data suggest that 2.18 mg/s flow results in the highest anode efficiency at all operating points except 180V. No pattern is clearly discernable from these results, and the measurement uncertainties limit the significance of any identified trends with respect to flow rate.

IV.Conclusions

A main goal of this work was to assess whether low-cost additive manufacturing processes such as FFF or 3D printing of glazed ceramics can be used in the fabrication of Hall effect thrusters. While the data collected cover only short duration testing, our results demonstrate that the UAH-78AM is capable of operating with in normal jet-mode Hall discharge with performance comparable to other thrusters of a similar power and size. Therefore, by the most basic definition, the UAH-78AM is a fully functioning Hall Thruster, and FFF and other low-cost additive manufacturing technologies can be used to build Hall thrusters.

However, for a Hall thruster to be useful, it must be capable of sustaining a Hall discharge for long enough duration to collect meaningful data or provide sustained thrust for satellites in flight applications. The acceptable running duration is dependent on the type of data being collected. In the case of the UAH-78AM, current test durations are too short to collect plume data or steady-state thrust and temperature data using conventional methods. The only measurements that can be collected with the UAH-78AM are transient, since the steady state thermal operating condition for the thruster is beyond the temperature limits of the materials used for the channel. While transient data might be insightful for baselining the performance of a thruster, steady state data is ultimately needed for the development of flight hardware.

Another important consideration is that thruster design deficiencies of the UAH-78AM could be contributing to the short test durations. Channel wall heating and erosion in Hall effect thrusters are dependent on the magnetic field topology in the channel. Magnetically shielded field topologies have been found to reduce channel wall heating by reducing the contact between the plasma and the wall [18,19]. Our magnetic circuit design was based on an unshielded field topology for the purpose of simplicity; however, the unshielded design only increases thermal losses to the channel walls as compared to shielded designs.

The heating and outgassing behavior of the polymer components have a distinct impact on the performance of the thruster and lead to a unique failure mechanism. The data suggest, but do not prove, that polymer outgassing contributes to an increase in thrust until spot formation. However, an analysis of species in the plume would be necessary to experimentally verify if polymer heating and outgassing are contributing to the positive thrust drift over the test duration. Plume properties and plasma-wall interactions in the thruster may be interesting areas for future research, since the 3D printed components in the thruster likely modify the channel wall sheaths and plume properties relative to conventional thrusters. It's likely that such modifications have a discernable impact on thruster performance but may be challenging to identify in transient testing.

Acknowledgments

The authors gratefully acknowledge the support of the electric propulsion team at NASA GRC in helping to solve the myriad of implementation and integration challenges associated with designing and testing Hall thrusters; it's been a pleasure working and learning with you.

In addition, student support for this research is funded through the Alabama Space Grant Fellowship Program under NASA Training Grant #NNX15AJ18H. The authors gratefully acknowledge the Alabama Space Grant Consortium for their financial contributions that support this research.

References

[1] Hall, S. J., Florenz, R. E., Gallimore, A., Kamhawi, H., Brown, D. L., Polk, J. E., Goebel, D. M., and Hofer, R. R., "Implementation and Initial Validation of a 100-kW Class Nested-channel Hall Thruster," *50th AIAA/ASME/SAE/ASEE Joint Propulsion Conference*, Cleveland, OH: American Institute of Aeronautics and Astronautics, 2014.

[2] J Ibarzo, I. Caro, J. Marcos, and J. Gonzalez Del Amo, "Alternative manufacture technologies for the manufacture of HET larger ceramic chamber," *The 32nd International Electric Propulsion Conference*, Wiesbaden, Germany: 2011.

[3] Joshi, S. C., and Sheikh, A. A., "3D printing in aerospace and its long-term sustainability," *Virtual and Physical Prototyping*, vol. 10, Oct. 2015, pp. 175–185.

[4] Dunaevsky, A., Raitses, Y., and Fisch, N. J., "Secondary electron emission from dielectric materials of a Hall thruster with segmented electrodes," *Physics of Plasmas*, vol. 10, Jun. 2003, pp. 2574–2577.

[5] Choueiri, E., "Fundamental difference between the two variants of Hall thrusters-SPT and TAL," *37th Joint Propulsion Conference and Exhibit*, Salt Lake City, UT: 2001, p. 3504.

[6] Dunaevsky, A., Raitses, Y., and Fisch, N. J., "Yield of Secondary Electron Emission From Ceramic Materials of Hall Thruster with Segmented Electrodes."

[7] Haas, J. M., "Low-Perturbation Interrogation of the Internal and Near-Field Plasma Structure of a Hall Thruster Using a High-Speed Positioning System," Ph.D. Dissertation, The Universtiy of Michigan, 2001.

[8] Conversano, R. W., Goebel, D. M., Hofer, R. R., Matlock, T. S., and Wirz, R. E., "Magnetically shielded miniature Hall thruster: development and initial testing," *33rd International Electric Propulsion Conference*, Washington, DC: 2013.

[9] Huber, C., Abert, C., Bruckner, F., Groenefeld, M., Muthsam, O., Schuschnigg, S., Sirak, K., Thanhoffer, R., Teliban, I., Vogler, C., Windl, R., and Suess, D., "3D print of polymer bonded rare-earth magnets, and 3D magnetic field scanning with an end-user 3D printer," *Applied Physics Letters*, vol. 109, Oct. 2016, p. 162401.

[10] Li, L., Tirado, A., Nlebedim, I. C., Rios, O., Post, B., Kunc, V., Lowden, R. R., Lara-Curzio, E., Fredette, R., Ormerod, J., Lograsso, T. A., and Paranthaman, M. P., "Big Area Additive Manufacturing of High Performance Bonded NdFeB Magnets," *Scientific Reports*, vol. 6, Dec. 2016.

[11] Ma, B. ., Herchenroeder, J. ., Smith, B., Suda, M., Brown, D. ., and Chen, Z., "Recent development in bonded NdFeB magnets," *International Symposium on Physics of Magnetic Materials/Internat ional Symposium on Advanced Magnetic Technologies*, vol. 239, Feb. 2002, pp. 418–423.

[12] Szabo, J. J., Pote, B., Tedrake, R., Paintal, S., Byrne, L., Hruby, V. J., Kamhawi, H., and Smith, T., "High Throughput 600 Watt Hall Effect Thruster for Space Exploration," *52nd AIAA/SAE/ASEE Joint Propulsion Conference*, 2016, p. 4830.

[13] Haag, T. W., "Thrust stand for high-power electric propulsion devices," *Review of Scientific Instruments*, vol. 62, May 1991, pp. 1186–1191.

[14] Martinez, R. A., Dao, H., and Walker, M. L. R., "Power Deposition into the Discharge Channel of a Hall Effect Thruster," *Journal of Propulsion and Power*, vol. 30, Jan. 2014, pp. 209–220.

[15] Hruby, V., Monheiser, J., Pote, B., Rostler, P., Kolencik, J., and Freeman, C., "Development of low power Hall thrusters," *30th Plasmadynamic and Lasers Conference*, 1999, p. 3534.

[16] Polk, J. E., Pancotti, A., Haag, T., King, S., Walker, M., Blakely, J., and Ziemer, J., "Recommended practices in thrust measurements," *The 33rd International Electric Propulsion Conference*, Washington, DC: 2013.

[17] Liz, P., and Vicki, B., *Preparaiton of Calibration Curves A Guide to Best Practices*, LGC/VAM, 2003.

[18] Hofer, R., Goebel, D., Mikellides, I., and Katz, I., "Design of a Laboratory Hall Thruster with Magnetically Shielded Channel Walls, Phase II: Experiments," American Institute of Aeronautics and Astronautics, 2012.

[19] Goebel, D. M., Hofer, R. R., Mikellides, I. G., Katz, I., Polk, J. E., and Dotson, B. N., "Conducting wall Hall thrusters," *IEEE Transactions on Plasma Science*, vol. 43, 2015, pp. 118–126.